New Repetitive Control with Improved Steady-state Performance and Accelerated Transient

Xu Chen and Masayoshi Tomizuka

Abstract—**In repetitive control, the enhanced servo performance at the fundamental frequency and its higher-order harmonics is usually followed by undesired error amplifications at other frequencies. In this paper, we discuss a new structural configuration of the internal model in repetitive control, wherein designers have more flexibility in the repetitive loop-shaping design, and the amplification of non-repetitive errors can be largely reduced. Compared to conventional repetitive control, the proposed scheme is especially advantageous when the repetitive task is subject to large amounts of non-periodic disturbances. An additional benefit is that the transient response of the plug-in repetitive control can be easily controlled, leading to an accelerated transient with reduced overshoots. Verification of the algorithm is provided by simulation of a benchmark regulation problem in hard disk drives, and by tracking-control experiments on a laboratory testbed of an industrial wafer scanner.**

Index Terms—**repetitive control, digital control, disturbance observer, transient control, internal model principle**

I. Introduction

Repetitive control (RC) is a well-known servo design tool for systems that are subjected to periodic disturbances/references. It implements an internal model [1] $1/(1-z^{-N})$ (N is the period of the disturbance/reference), or $1/(1-e^{-T_p s})$ in the continuous-time case (T_p denotes the period), into a feedback system, such that errors in the previous repetition can be used to improve the current regulation/tracking control. Distinguished by its high performance as well as the simple design and implementation criteria, ever since its introduction [2]–[4], RC has attracted a great amount of research efforts [3]–[6]. Its versatility has been tested in various practical applications, including but not limited to: track-following in magnetic and optical disk drives [7]–[10], robot arm control [11], and regulation control in vehicles [12]. For more complete lists of applications, readers can refer to the survey papers [5], [6].

The configuration of the internal model and its interaction with the feedback system vary in literature. The continuous-time RC design mainly applies a series or parallel plug-in configuration [3], [8], [13]–[16]. The prototype RC [4], [17] applies the Zero-Phase-Error-Tracking [18] idea and directly cascades a robust version of $1/(1-z^{-N})$ into the open-loop transfer function. Additionally there are plug-in configurations of discrete RC design, among which [19], [20] applied optimization techniques with an extended high-order internal model.

Ultimately, a generalized version of $1-z^{-N}$ or $1-e^{-T_p s}$ is absorbed into the denominator of the overall feedback controller, therefore creating high-gain control at the repetitive frequencies (frequencies of the roots of $1-z^{-N}=0$ or $1-e^{-T_p s}=0$).[1] From Bode's Integral Theorem (see, e.g., [21]), enhanced servo performance at certain frequencies commonly results in deteriorated loop shapes at other frequencies. This fundamental limitation, reflected in repetitive control, is the comb-like magnitude response in the closed-loop sensitivity function, along with undesired gain amplifications at frequencies other than the comb centers (see some examples in [8], [13], [15], [16], [19], [20]). The problem is more significant if there are large non-periodic components in the disturbance (e.g., in hard disk drive systems [22]).

Relaxing the previous performance limitations, this paper proposes a new structural RC design with improved loop-shaping properties. Instead of using the full information of the previous errors, we provide an approach to extract only the repetitive errors in feedback control. In the frequency domain, this corresponds to a series-parallel implementation of the internal model with direct control of the comb-like loop shape, leading to greatly reduced gain amplifications at the non-repetitive frequencies. An additional benefit of the reduced gain amplification is that the proposed design shows increased ability to reject repetitive errors at high frequencies. A second contribution of the paper is to provide a generalized concept of the disturbance observer (DOB) [23], which has been well-known as a robust control design tool [24]–[28] but, to the authors' best knowledge, has not been discussed in a general context for repetitive control. Finally, we discuss a flexible control of the transient performance in RC, leading to a smoother and accelerated transient response. A short version of the

Manuscript received February 14, 2012; revised September 11, 2012; accepted March 10, 2013. Manuscript received in final form March 13, 2013. This work was supported in part by the Computer Mechanics Laboratory (CML) in the Department of Mechanical Engineering, University of California, Berkeley.

The authors are with the Department of Mechanical Engineering, University of California, Berkeley, CA, 94720, USA (email: maxchen@me.berkeley.edu; tomizuka@me.berkeley.edu)

[1] i.e., kF_s/N Hz for $1-z^{-N}=0$ and k/T_p Hz for $1-e^{-T_p s}=0$. Here $k=0,1,2,...$ and F_s is the sampling frequency. F_s/N and $1/T_p$ are called the fundamental frequencies.

paper appeared in [29]. The added values here include: detailed proof and analysis that are omitted from the conference version (especially in Sections II and V); additional discussion of the transient design in Sections V and VI; experimental results; and the newly developed Section III.

The remainder of the paper is organized as follows. Sections II and IV present the proposed controller design and the stability conditions. Section III provides a detailed comparison of the proposed algorithm with related prior publications. In Section V, we discuss the reduction of overshoot and transient time when implementing the add-on compensator. Section VI provides verification of the algorithm by simulation and experimentation. Section VII concludes the paper.

II. Controller parametrization

Fig. 1 presents the proposed closed-loop repetitive control scheme. Here $P(z^{-1})$ is the sampled plant (with digital holders) to be controlled. $C(z^{-1})$ is an existing feedback controller designed by any proper loop-shaping methods (e.g., PID or H_∞ control) to achieve the baseline servo performance and robustness. The signals $r(k)$, $y(k)$, $u(k)$, and $d(k)$ are respectively the reference, the plant output, the control input, and the lumped input disturbance.

The proposed plug-in RC design utilizes the internal signals $e(k)$ and $u(k)$ to generate a compensation signal $c(k)$ in Fig. 1. In the case of regulation control, $r(k) = 0$; we aim to have $c(k)$ cancel the *periodic components* in $d(k)$. In the tracking-control case, $c(k)$ functions to reduce the tracking error between $y(k)$ and the non-zero periodic $r(k)$.

Within the plug-in compensator we have three modules:

- z^{-m}, where m denotes the relative degree of $P(z^{-1})$;
- $P_n^{-1}(z^{-1})$–a nominal model of $z^{-m}P^{-1}(z^{-1})$;
- and $Q(z^{-1})$–a filter to be designed shortly.

Notice that $P^{-1}(z^{-1})$ may be anti-causal but we have added delays such that $P_n^{-1}(z^{-1})$ is realizable in Fig. 1.

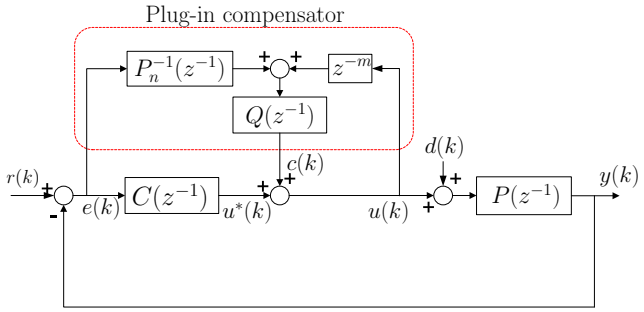

Figure 1: Block diagram of the proposed repetitive control scheme.

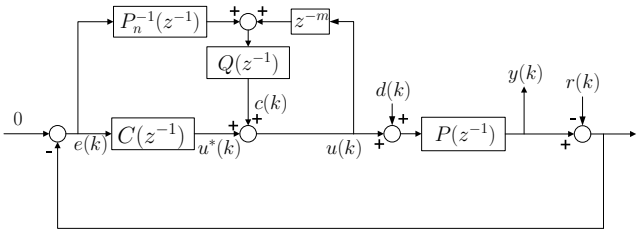

(a) Equivalent form of Fig. 1.

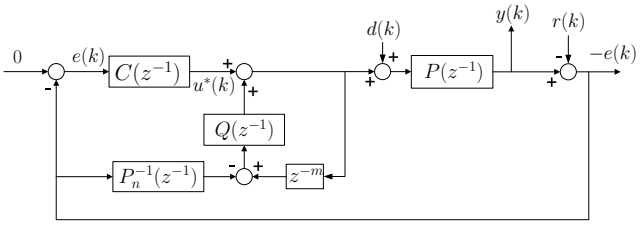

(b) Equivalent form of Fig. 2a.

Figure 2: Block diagram transformation for converting Fig. 1 to Fig. 3.

A. Time-domain analysis

Notice that if the $P_n^{-1}(z^{-1})$ block is removed from Fig. 1 and $Q(z^{-1})$ is set to $z^{-(N-m)}$, the open-loop transfer function becomes $P(z^{-1})\frac{1}{1-z^{-N}}C(z^{-1})$, and the proposed compensator reduces to an ideal-case plug-in repetitive controller that is similar to prior constructions. To see the intuition of the proposed scheme and the design of $Q(z^{-1})$, we first transform the block diagram to a repetitive disturbance observer (RDOB) scheme. Notice that for either regulation or tracking control, RC aims at maintaining $e(k)$ small. Performing the block diagram transformations in Fig. 2, we obtain a unified regulation problem in Fig. 3, where $-e(k)$ can be regarded as a fictitious output that is regulated in the presence of the equivalent disturbances $d(k)$ and $r(k)$.

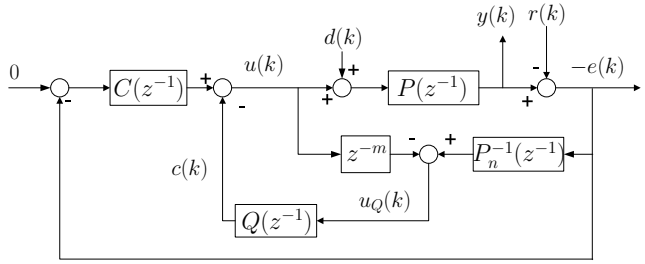

Figure 3: Equivalent scheme of Fig. 1, from the perspective of a repetitive disturbance observer.

In Fig. 3, consider first the case where $r(k) = 0$ (regulation problem for rejecting repetitive disturbances). Since $y(k) = P(z^{-1})(u(k) + d(k))$, the output of $P_n^{-1}(z^{-1})$ is given by $P_n^{-1}(z^{-1})P(z^{-1})(u(k)+d(k))$. Notice that $P_n^{-1}(z^{-1}) \approx z^{-m}P^{-1}(z^{-1})$. Through the inverse filtering, the output of $P_n^{-1}(z^{-1})$ thus approximately equals $u(k-m) + d(k-m)$. Subtracting now $u(k-m)$, the output of the z^{-m} block, yields an approximated $d(k-m)$ (i.e., $u_Q(k) = \hat{d}(k-m)$).

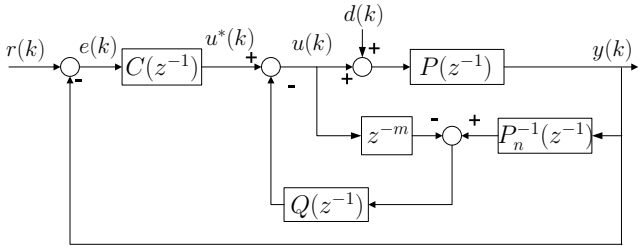

Figure 4: Block diagram of a conventional disturbance observer.

Due to the m-step delays, the non-repetitive components in $d(k)$, and the unavoidable modeling errors in $P_n^{-1}(z^{-1})$, directly applying $\hat{d}(k-m)$ to cancel $d(k)$ commonly gives poor performance (consider a simple example where $P(z^{-1}) = z^{-2}(1+\Delta)$; Δ is the model uncertainty). The idea of the proposed RDOB is to first obtain this estimated $d(k-m)$ via the preceding filtering, and then apply a Q filter that aims at extracting only the repetitive components and counteracting the m-step delay effect. This intuition applies also to the case when $r(k) \neq 0$ (in repetitive reference tracking), where analogous analysis gives that the output of $Q(z^{-1})$ is an approximation of $-P^{-1}(z^{-1})r(k)$.

Compared to a conventional DOB-based servo control in Fig. 4 (see e.g., [26], [27], [30]), Fig. 3 differs in two aspects. First, we directly treat the repetitive reference $r(k)$ as an output disturbance for $e(k)$. This changes the $r(k)$-to-$e(k)$ transfer function from $(1-z^{-m}Q+PP_n^{-1}Q)/(1+PC+(PP_n^{-1}-z^{-m})Q)$ in Fig. 4 to $(1-z^{-m}Q)/(1+PC+(PP_n^{-1}-z^{-m})Q)$ (derivations provided in the next subsection) in Fig. 3, and makes the proposed scheme suitable for both regulation and tracking problems. Second, the central component $Q(z^{-1})$ is a repetitive-signal extractor rather than a lowpass filter, yielding the fundamentally different loop shapes and design criteria for repetitive control.

B. Repetitive loop shaping

From Fig. 1, the equivalent controller from $e(k)$ to $u(k)$ is

$$C_{eq}(z^{-1}) = \frac{C(z^{-1}) + Q(z^{-1})P_n^{-1}(z^{-1})}{1 - z^{-m}Q(z^{-1})}, \tag{1}$$

from which we can obtain the sensitivity function $S = 1/(1+PC_{eq})$ (for the sake of brevity, we omit the z-domain index z^{-1} here):

$$S = \frac{1 - z^{-m}Q}{1 + PC + (PP_n^{-1} - z^{-m})Q}. \tag{2}$$

The closed-loop transfer functions from $d(k)$ and $r(k)$ to $e(k)$ are respectively given by

$$G_{ed}(z^{-1}) = -P(z^{-1})S(z^{-1}) \tag{3}$$

$$G_{er}(z^{-1}) = S(z^{-1}). \tag{4}$$

Notice that in regions where the frequency response $P(e^{-j\omega})$ is well modeled by $e^{-jm\omega}P_n(e^{-j\omega})$, we have $P(z^{-1})P_n^{-1}(z^{-1}) - z^{-m} \approx 0$ (in the frequency domain) such that the sensitivity function in (2) satisfies

$$S(z^{-1}) \approx \frac{1 - z^{-m}Q(z^{-1})}{1 + P(z^{-1})C(z^{-1})}. \tag{5}$$

In the frequency regions where large model mismatch exists, we will make $|Q(e^{-j\omega})|$ small such that the contribution of $[P(z^{-1})P_n^{-1}(z^{-1}) - z^{-m}]Q(z^{-1})$ in (2) is still insignificant to make (5) a valid approximation.

By the above constructions, we have separated the baseline system response $1/(1+P(z^{-1})C(z^{-1}))$ from $S(z^{-1})$ in (5), and can now focus on designing the term $1 - z^{-m}Q(z^{-1})$, to introduce the desired regulation/tracking performance. The use of the inverse model $P_n^{-1}(z^{-1})$ has helped to make this added module $1-z^{-m}Q(z^{-1})$ simple and depend little on the dynamics of $P(z^{-1})$ (only the plant delay z^{-m} appears here).

Assume the disturbance contains only repetitive components that asymptotically satisfy the internal model

$$(1 - z^{-N})d(k) = 0, \tag{6}$$

or in the tracking-control case

$$(1 - z^{-N})r(k) = 0. \tag{7}$$

From (3) and (4), to reject $d(k)$ and $r(k)$, it suffices to have $S(z^{-1})d(k)$ and $S(z^{-1})r(k)$ converge asymptotically to zero. By combining (2), (6) and (7), one may notice that this sufficient condition is achieved if $1-z^{-m}Q(z^{-1})$ contains the term $1-z^{-N}$. Assigning $Q(z^{-1}) = z^{-(N-m)}$ is one way which gives a scheme similar to conventional RC. In this paper we propose to apply an Infinite Impulse Response (IIR) Q filter satisfying

$$Q(z^{-1}) \triangleq \frac{B_Q(z^{-1})}{A_Q(z^{-1})}$$

and

$$A_Q(z^{-1}) - z^{-m}B_Q(z^{-1}) = 1 - z^{-N}. \tag{8}$$

Designing

$$A_Q(z^{-1}) = 1 - \alpha^N z^{-N} \tag{9}$$

and solving (8) yield

$$B_Q(z^{-1}) = (1-\alpha^N)z^{-(N-m)} \tag{10}$$

$$1 - z^{-m}Q(z^{-1}) = \frac{1 - z^{-N}}{1 - \alpha^N z^{-N}}. \tag{11}$$

Hence we have achieved to include the $1-z^{-N}$ numerator in $1-z^{-m}Q(z^{-1})$, with an additional tunable module $1-\alpha^N z^{-N}$. Here $\alpha(\in[0,1])$ is the ratio between magnitudes of the poles and the zeros in $1-z^{-m}Q(z^{-1})$.[2] If $\alpha = 0$, $Q(z^{-1})$ becomes a Finite Impulse Response (FIR) filter ($Q(z^{-1}) = z^{-N+m}$) and RDOB generates a loop shape that is similar to prior publications. This will be discussed

[2]For this analytical reason, we used α^N instead of defining $A_Q(z^{-1}) = 1-\beta z^{-N}$ in (9), to avoid the appearance of (numerically more fragile) $\sqrt[N]{\cdot}$ in our discussion. Yet for practical implementation, $\beta \triangleq \alpha^N$ can directly be used without the need of computing α^N online.

in more details in Section III. On the other hand, $\alpha = 1$ cuts off the repetitive compensation. When $\alpha \in [0,1)$, the loop shape can be flexibly designed. For instance, let $N = 10$, $m = 1$, and assume a sampling frequency of 26400 Hz. Increasing α from 0 to 0.99 yields the magnitude responses in Fig. 5. We observe from the top plot that, as α increases towards 1 (while still satisfying $\alpha \in [0,1)$), $1 - z^{-m}Q(z^{-1})$ has a sharper comb-like magnitude response and a smaller H_∞ norm. Correspondingly in the bottom plot, $Q(z^{-1})$ behaves as a sharper spectral-selection filter to preserve only the repetitive components. Specifically, if $\alpha = 0$, $Q(z^{-1})$ has a magnitude response valued always at 1, and both the repetitive and the non-repetitive error components are directly used for feedback compensation; in the mean time, the maximum value of $1 - z^{-m}Q(z^{-1})$ equals $\left\|1 - z^{-m}z^{-(N-m)}\right\|_\infty = 2$, i.e., disturbances at the corresponding frequencies get amplified by 100%. One can observe that the design of (9) and the introduction of α have provided an additional degree of freedom for repetitive loop shaping, enabling the improvement in Fig. 5, from the solid lines to the dotted lines. Additionally we have the following theorem:

Theorem 1: When $P(z^{-1}) = z^{-m}P_n(z^{-1})$, conventional RC amplifies non-repetitive disturbances by 100% in the worst case. The worst-case amplification is $\left(2/(1+\alpha^N) - 1\right) \times 100\%$ in the proposed scheme. The maximum amplification occurs to the disturbance components at the frequencies $(2k+1)/(2T_sN)$ Hz, $k = 0,1,\ldots$.

Proof: The maximum disturbance amplification corresponds to the maximum magnitude response of $1 - z^{-m}Q(z^{-1})$ in (2). For (11), the *squared* magnitude response is

$$\frac{1-e^{-j\omega N}}{1-\alpha^N e^{-j\omega N}} \times \frac{1-e^{j\omega N}}{1-\alpha^N e^{j\omega N}} = \frac{1-\cos(\omega N)}{\frac{1+\alpha^{2N}}{2} - \alpha^N \cos(\omega N)} \tag{12}$$

where $\omega = 2\pi\Omega_{Hz}T_s$ (Ω_{Hz} is in Hz, T_s is the sampling time in sec).

Noting, $\cos(\omega N) \in [-1,1]$, we need only consider the behavior of the function

$$f(x) = \frac{1-x}{\frac{1+\alpha^{2N}}{2} - \alpha^N x},\ x \in [-1,1].$$

The derivative of $f(x)$ is

$$f'(x) = \frac{-\frac{1}{2}(1-\alpha^N)^2}{\left(\frac{1+\alpha^{2N}}{2} - \alpha^N x\right)^2},\ x \in [-1,1].$$

It is straightforward to see that $f'(x)$ monotonically decreases as x increases from -1 to 1. Thus, $\min\{f(x)\}$ and $\max\{f(x)\}$ are attained respectively at $x = 1$ and $x = -1$, with $\min\{f(x)\} = 0$ and

$$\|1 - z^{-m}Q(z^{-1})\|_\infty^2 = \max\{f(x)\} = \left(\frac{2}{1+\alpha^N}\right)^2. \tag{13}$$

Taking the square root of (13) gives the maximum amplification gain. Solving $x = \cos(2\pi\Omega_{Hz}T_sN) = -1$ gives that the maximum occurs at the frequencies $\Omega_{Hz} = (2k+1)/(2T_sN)$, $k = 0,1,\ldots$. As a special case of $\alpha = 0$ (conventional RC), $\|1 - z^{-m}Q(z^{-1})\|_\infty = \sqrt{\max\{f(x)\}\big|_{\alpha=0}} = 2$. The proof is done by computing the relative amplification $(\|1 - z^{-m}Q\|_\infty - 1) \times 100\%$. ■

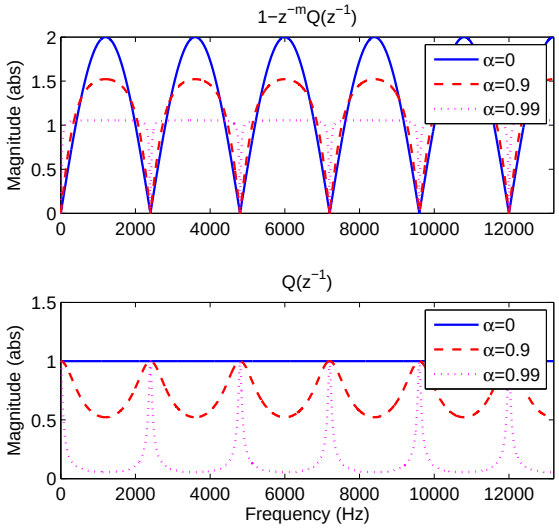

Figure 5: Magnitude responses of $1 - z^{-m}Q(z^{-1})$ and $Q(z^{-1})$ with different values of α.

Notice that Bode's Integral Theorem still holds. Reduced amplifications of the non-repetitive errors are accompanied with smaller regions of repetitive-error rejection in Fig. 5. Correspondingly, sensitivity of the algorithm w.r.t. the repetitive frequencies is increased.

C. Robustness and implementation of $Q(z^{-1})$

One central assumption in the previous subsection is the small gain of $\left[P(z^{-1})P_n^{-1}(z^{-1}) - z^{-m}\right]Q(z^{-1})$ in (2). It is practically not possible to have a perfectly accurate model of $P(z^{-1})$ in the high-frequency region, and thus necessary to incorporate a lowpass filter in $Q(z^{-1})$ to make the influence of $\left[P(z^{-1})P_n^{-1}(z^{-1}) - z^{-m}\right]Q(z^{-1})$ small. In the context of repetitive control, it is additionally possible (and recommended) to apply a zero-phase lowpass filter. One simple and flexible construction is proposed as follows. Define first the following zero-phase lowpass filter as a base structure

$$q_0(z,z^{-1}) = \frac{(1+z^{-1})^{n_0}(1+z)^{n_0}}{4^{n_0}} \tag{14}$$

where $2n_0$ is the number of placed zeros at the Nyquist frequency. To have additional freedom on the cut-off frequency, we can add extra zero-phase pairs given by

$$q_i(z,z^{-1}) = q_i(z^{-1})q_i(z), \tag{15}$$

$$q_i(z^{-1}) = \frac{1 - 2\cos(\omega_i T_s)z^{-1} + z^{-2}}{2 - 2\cos(\omega_i T_s)}. \tag{16}$$

Here i is the index number; ω_i is in rad/sec. The filter $q_i(z,z^{-1})$ places four zeros at $e^{\pm\omega_i T_s}$ to remove the frequency components at ω_i's rad/sec, and is normalized by

$(2-2\cos(\omega_i T_s))^2$ to have a unity DC gain. The zero-phase property is preserved since the frequency responses of $q_i(z^{-1})$ and $q_i(z)$ are complex conjugates of each other.

Defining $q(z,z^{-1}) = \prod_j q_j(z,z^{-1})$, we can now construct the practical version of $Q(z^{-1})$:

$$Q(z^{-1}) = \frac{(1-\alpha^N)z^{-(N-m-n_q)}}{1-\alpha^N z^{-N}} z^{-n_q} q(z,z^{-1}) \qquad (17)$$

where n_q is the highest order of z in $q(z,z^{-1})$ (so that $z^{-n_q}q(z,z^{-1})$ is realizable). It can be noted that $Q(z^{-1})$ is causal as long as $N-m-n_q \geq 0$. Fig. 6 presents one realization of (17), with N memory elements for the repetitive signal generator. The bandwidth of the low-pass filter $q(z,z^{-1})$ can roughly be tuned by comparing the magnitude responses of $\left[P(z^{-1})P_n^{-1}(z^{-1}) - z^{-m}\right]Q(z^{-1})$ and $1+P(z^{-1})C(z^{-1})$. A more strict constraint from the stability criteria will be provided in Section IV.

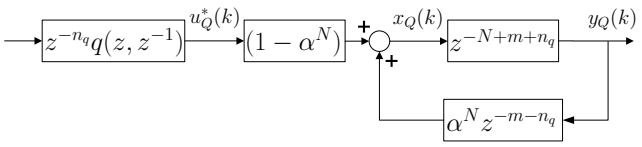

Figure 6: Implementation of the Q filter.

D. The plant and its inverse

In Fig. 1, stability of $P_n^{-1}(z^{-1})$ is required for internal stability. If $P_n(z^{-1})$ is a minimum-phase system, $P_n^{-1}(z^{-1})$ can directly be used. For a practical sampled-data system, non-minimum phase zeros may occur in $P(z^{-1})$ (usually in the high-frequency region [31], [32]). If this happens, the Zero-Phase-Error-Tracking (ZPET) algorithm [18] can be used to obtain a stable $P_n^{-1}(z^{-1})$.

An additional concern for $P(z^{-1})$ is the possible appearance of resonances in the high-frequency region. In this case, one can extend $P(z^{-1})$ to include the baseline anti-resonance controllers (e.g., notch filters), yet with a possible increase of m in $P_n^{-1}(z^{-1}) \approx z^{-m}P^{-1}(z^{-1})$, due to the phase loss in anti-resonance design.

III. Connections with prior schemes

With (17), the equivalent feedback controller in (1) is

$$C_{eq} = \frac{q(z,z^{-1})(1-\alpha^N)z^{-(N-m)}P_n^{-1} + (1-\alpha^N z^{-N})C}{1-\left[1-(1-\alpha^N)(1-q(z,z^{-1}))\right]z^{-N}}.$$

For the ideal case of $q(z,z^{-1}) = 1$ (perfect disturbance rejection), $C_{eq} = \left[(1-\alpha^N)z^{-(N-m)}P_n^{-1} + (1-\alpha^N z^{-N})C\right]/(1-z^{-N})$. One can remark that the internal model is absorbed in the loop in a series-parallel fashion (the two terms in the numerator of C_{eq} are in parallel form, and the common part $1/(1-z^{-N})$ is in series with them).

Table I summarizes the equivalent overall feedback controllers in different repetitive-control schemes. The ideal forms in the second and the third columns provide perfect disturbance rejection but are highly sensitivity to model mismatches. Lowpass filters in the form of $q(z,z^{-1})$ or $q(s)$ are used in the robust versions. $C(z^{-1})$ and $C(s)$ denote the baseline feedback controllers. On the fourth line of Table I, $P_{ZPET}^{-1}(z^{-1})$ in prototype RC denotes the ZPET inverse [18] that approximates $P^{-1}(z^{-1})$.

Several connections can be made from Table I. First, comparing "Prototype RC" with "Proposed RDOB with an FIR Q", we can observe that the former can be regarded as a special case of the latter with $C(z^{-1}) = 0$ and $z^m P_n^{-1}(z^{-1}) = P_{ZPET}^{-1}(z^{-1})$. Second, if we replace $z^{-(N-m)}P_n^{-1}(z^{-1})$ with $P^{-1}\sum_m w_m z^{-mN}$ and let $C(z^{-1}) := C_o(z^{-1})\sum_m w_m z^{-mN}$, then the high-order RC can be realized in a similar fashion as the proposed RDOB with an FIR Q filter.

It can now be seen that with an *FIR* Q filter, the proposed RDOB has close connections with prior RC schemes. From the second and the third rows of Table I, an IIR Q provides a different integration of the internal model and introduces the additional design freedom of α.

IV. Stability and robust stability

From the previous discussions, if $P_n^{-1}(z^{-1})$ and $Q(z^{-1})$ are properly designed, the sensitivity function in (2) approximates $(1-z^{-m}Q(z^{-1}))/(1+P(z^{-1})C(z^{-1}))$, and the closed-loop stability is preserved. Strict nominal closed-loop stability is obtained by using (1) and computing the roots of the characteristics equation from $1+P(z^{-1})C_{eq}(z^{-1}) = 0$.

When the plant is perturbed to be $\tilde{P}(z^{-1}) = P(z^{-1})(1+\Delta(z^{-1}))$ (assume the uncertainty $\Delta(z^{-1})$ is stable and has a bounded H_∞ norm), applying the Small Gain Theorem (see, e.g., [21]) yields the following robust-stability condition:

$$\left\|\Delta(z^{-1})T(z^{-1})\right\|_\infty < 1 \qquad (18)$$

where the complementary sensitivity function $T = PC_{eq}/(1+PC_{eq})$ is given by, after substituting in (1) and simplification,

$$T = \frac{CP + P_n^{-1}PQ}{1+CP+Q(P_n^{-1}P - z^{-m})}.$$

Notice that to avoid conservativeness, we perturbed the plant w.r.t. $P(z^{-1})$ instead of $z^{-m}P_n(z^{-1})$, since from Section II-D the latter term may already contain reduced information compared to $P(z^{-1})$. An example of robust stability analysis is provided in Fig. 10.

V. Transient response and algorithm implementation

With the plug-in compensator, a new feedback system is formed. The plug-in repetitive controller may be turned on or off depending on the presence of repetitive disturbances. Although the two closed loops are designed to be asymptotically stable, switching between the two stabilizing controllers in general does not yield smooth response [34]. To be more specific for the plug-in

Table I: Equivalent feedback controllers in repetitive control schemes

	Ideal form	(expanded) Ideal form	Robust version
Proposed RDOB w/ an IIR Q	$\frac{C(z^{-1})+P_n^{-1}(z^{-1})Q(z^{-1})}{1-z^{-m}Q(z^{-1})}$, $Q(z^{-1})=\frac{(1-\alpha^N)z^{-N+m}}{1-\alpha^N z^{-N}}$	$\frac{(1-\alpha^N)z^{-(N-m)}P_n^{-1}(z^{-1})+(1-\alpha^N z^{-N})C(z^{-1})}{1-z^{-N}}$	$\frac{q(z,z^{-1})(1-\alpha^N)z^{-(N-m)}P_n^{-1}(z^{-1})+(1-\alpha^N z^{-N})C(z^{-1})}{1-\left[1-(1-\alpha^N)(1-q(z,z^{-1}))\right]z^{-N}}$
Proposed RDOB w/ an FIR Q	$\frac{C(z^{-1})+P_n^{-1}(z^{-1})Q(z^{-1})}{1-z^{-m}Q(z^{-1})}$, $Q(z^{-1})=z^{-N+m}$	$\frac{z^{-(N-m)}P_n^{-1}(z^{-1})+C(z^{-1})}{1-z^{-N}}$	$\frac{q(z,z^{-1})z^{-(N-m)}P_n^{-1}(z^{-1})+C(z^{-1})}{1-q(z,z^{-1})z^{-N}}$
Prototype RC [4], [17]	$\frac{k_r z^{-N}}{1-z^{-N}}P_{ZPET}^{-1}(z^{-1})$, $k_r\in(0,2)$	$\frac{k_r z^{-N}}{1-z^{-N}}P_{ZPET}^{-1}(z^{-1})$	$\frac{k_r q(z,z^{-1})z^{-N}}{1-q(z,z^{-1})z^{-N}}P_{ZPET}^{-1}(z^{-1})$
Plug-in RC [3], [8], [13]–[16], [33]	$C(s)(1+F(s)\frac{e^{-T_p s}}{1-e^{-T_p s}})$, $F(s)$ differs in specific papers.	$C(s)\frac{(1-e^{-T_p s})+F(s)e^{-T_p s}}{1-e^{-T_p s}}$	$C(s)\frac{(1-q(s)\cdot e^{-T_p s})+q(s)F(s)\cdot e^{-T_p s}}{1-q(s)\cdot e^{-T_p s}}$
High-order RC [19], [20]	$\frac{C(z^{-1})T_n^{-1}(z^{-1})\sum_m w_m z^{-mN}}{1-\sum_m w_m z^{-mN}}$, $T_n\approx\frac{P(z^{-1})C(z^{-1})}{1+P(z^{-1})C(z^{-1})}$	$\frac{(P^{-1}(z^{-1})+C(z^{-1}))\sum_m w_m z^{-mN}}{1-\sum_m w_m z^{-mN}}$	$\frac{C(z^{-1})T_n^{-1}(z^{-1})(\sum_m w_m z^{-mN})q(z,z^{-1})}{1-(\sum_m w_m z^{-mN})q(z,z^{-1})}$

repetitive control, we note that Fig. 6 has the following state-space realization

$$x_Q(k)=(1-\alpha^N)u_Q^*(k)+\alpha^N x_Q(k-N)$$
$$y_Q(k)=x_Q(k-N+m+n_q)$$

where $u_Q^*(k)$, $y_Q(k)\in\mathbb{R}$, and $x_Q(k)\in\mathbb{R}^N$. Notice that N, the period of the repetitive disturbance/reference, can be large. Correspondingly in this case, α^N can be quite small. When $x_Q(k)$ is initialized to zero, the first $N-m-n_q$ values of $y_Q(k)$ equal zero. Starting from the time instant $N-m-n_q+1$, $y_Q(N-m-n_q+i)=(1-\alpha^N)u_Q^*(i)$ for $i\in[1,N]$. At this first period of actual compensation, depending on the baseline closed-loop dynamics, the impulse of $u_Q^*(k)$ can create high-amplitude transient response in the error signal. Additionally, all the information in $u_Q^*(k)$, including the non-repetitive components, are fed back by the compensation signal $c(k)$ in Fig. 3, yielding mismatched cancellation for the non-periodic errors.

To reduce the possible overshoot and amplification of non-repetitive components, we can apply a time-varying α for transient improvement. It is proposed to initialize α at 1, and gradually reduce it to a designed value α_{end} (from steady-state analysis), following the decay rule

$$\alpha(k+1)=\alpha_{end}-(\alpha_{end}-\alpha(k))\alpha_{rate}, \tag{19}$$

with $\alpha(0)=1$ and the decay rate $\alpha_{rate}\in(0,1)$. Notice that when $\alpha=1$, the Q filter is essentially turned off in (17). By the above construction, at the first period of compensation, u_Q^* is gradually (weighted by $1-\alpha^N$) released to y_Q.

As for the settling time of the Q filter, the transient duration is determined by the pole location of the filter. Let n_t denote the number of periods for the impulse response of $Q(z^{-1})$ to reduce to less than 36.8% ($\approx e^{-1}$) of its peak value. From (17), this time constant is determined by $(\alpha^N)^{n_t}=e^{-1}$, i.e.,

$$n_t=\frac{-1}{\log\alpha^N}. \tag{20}$$

Here we allow non-integer value of n_t (e.g., $n_t=0.5$ means that it takes half the time of a period to settle).

From (20), the smaller the term α^N, the shorter the settling time. In the case that $\alpha=0$, $\lim_{\alpha\to 0}(n_t)=0$.

Combining the above discussion with that of Fig. 5, we can obtain in Table II the influence of α on various closed-loop properties. Notice the two conflicting objectives of maintaining (a) short transient duration and (b) small transient overshoot as well as good steady-state performance. Initializing α at 1 keeps the transient smooth and gradually reducing it afterward helps to accelerate the transient. Yet to maintain the steady-state performance, the final value of α may be required to be not too small. A slightly more complicated design of α is to first reduce it from 1 to a middle value α_{mid} and then increase it to a final α_{end}.

In summary, the following design procedures are suggested for implementing the proposed algorithm:

1) analyze the plant; obtain z^{-m} and $P_n^{-1}(z^{-1})$ according to Section II-D.
2) *design for steady-state performance according to Sections II-B and II-C*: obtain (17), check the frequency responses of $1-z^{-m}Q(z^{-1})$ and $S(z^{-1})$ (from (11) and (2) respectively); compute the maximum amplification from Theorem 1. Here it is suggested to start with an α that is close to unity (this gives smaller amplification of non-repetitive errors), and alter the value if stability or the desired performance metric is not reached.
3) *transient improvement*: compute (20) and simulate the time-domain closed-loop response–if large overshoot occurs, consider the time-varying α and initialize it at 1 as discussed in this section; if transient is excessively long, choose an intermediate value for α that is smaller than its steady-state value; keep the final value of α the same as the one designed in step 2).

A detailed design example is provided in Section VI.

VI. Case studies

A. Application to regulation control on a hard disk drive

This section provides a design example in the track-following control of a hard disk drive (HDD) system. In

Table II: The influence of α on the transient and the steady-state performance

value of $\alpha(\in [0,1])$	steady-state performance	transient overshoot	transient duration
large	small amplification of non-repetitive components	small	long
small	converse of the above	possibly large	short

this regulation-control example, the disk has a rotation speed of 7200 revolutions per minute (rpm), and the regulation control aims at positioning the read/write heads to follow the data tracks as precisely as possible. We implement the proposed algorithm to the HDD benchmark problem [35], where the plant is a 14-order system consisting of the dynamics of the power amplifier, the voice-coil motor, and the actuator mechanics. The input and the output of the plant correspond respectively to the (weighted) force input and the position of the read/write heads. At every revolution of the disks, 220 measurements are obtained, at a sampling frequency of 26400 Hz. The period of the repeatable disturbance is thus $N = 220$, at a fundamental frequency of $7200/60 = 120$ Hz. The baseline controller is a PID controller with several notch filters. The resulting baseline feedback system has gain and phase margins respectively of 5.45 dB and 38.2 deg, and an open loop servo bandwidth of 1.19 kHz.

In the RDOB design, we model $P(z^{-1})$ to contain the plant as well as the notch filters. Fig. 7 shows the frequency responses of $P(z^{-1})$ and $z^{-m}P_n(z^{-1})$ ($m = 2$ in this example). Since modeling errors appear after around 2 kHz, the zero-phase lowpass filter in Section II-C is designed to have a cut-off frequency of 2025 Hz, with $n_0 = 1$ in (14); $\omega_1 = 2\pi \times 122000$ rad/sec and $\omega_2 = 2\pi \times 8400$ rad/sec in (16). In view of the large value of N, α is designed to be 0.999 to achieve good steady-state performance. Correspondingly, α^N becomes 0.8024. α^N is directly implemented instead of α.

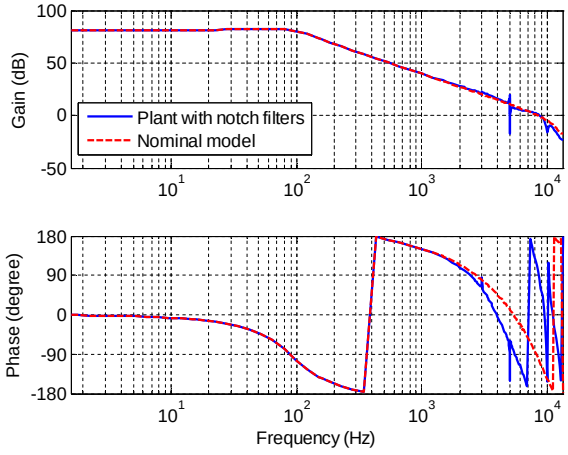

Figure 7: Frequency responses of $P(z^{-1})$ and $z^{-m}P_n(z^{-1})$.

The magnitude responses of $Q(z^{-1})$ and $1 - z^{-m}Q(z^{-1})$ are plotted respectively in the bottom and the top plots of Fig. 8. Notice the repetitive spectral-selection property (at multiples of the fundamental frequency 120 Hz) in $Q(z^{-1})$. This indicates that the repetitive disturbance observer only "observes" the periodic components and filters out the non-repetitive noise in the disturbance estimation.[3] For robustness, the zero-phase lowpass filter keeps the Q-filter gain small at high frequencies, yielding the gradual reduction of compensation capacity at high frequencies in $1 - z^{-m}Q(z^{-1})$. The magnitude responses of the actual closed-loop sensitivity functions are shown in Fig. 9. We can see that the designed loop shape in $1 - z^{-m}Q(z^{-1})$ is successfully transformed to the closed-loop system (recall the loop-shaping criterion (5)), and that the loop shapes at the non-repetitive frequencies are preserved in Fig. 9. The loop-shaping results can be compared with those in [15], [16], [19].

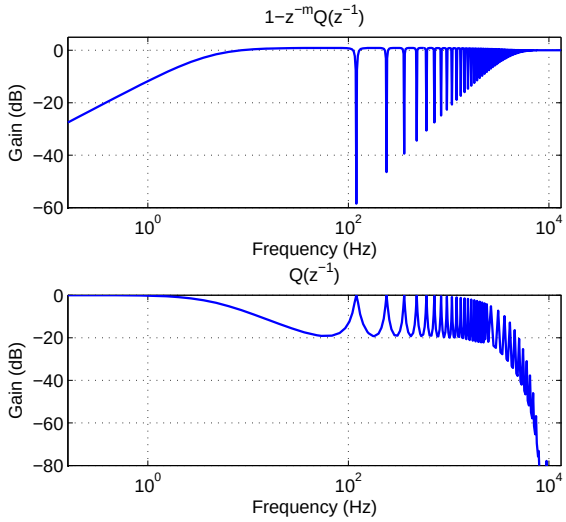

Figure 8: Magnitude responses of $1 - z^{-m}Q(z^{-1})$ and $Q(z^{-1})$.

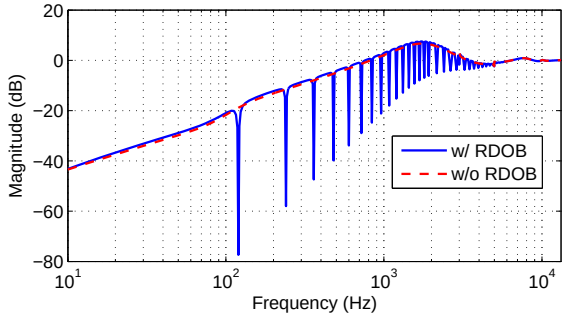

Figure 9: Magnitude responses of the sensitivity functions with and without the proposed RDOB.

[3]Note that a constant disturbance is also repetitive and observed by $Q(z^{-1})$.

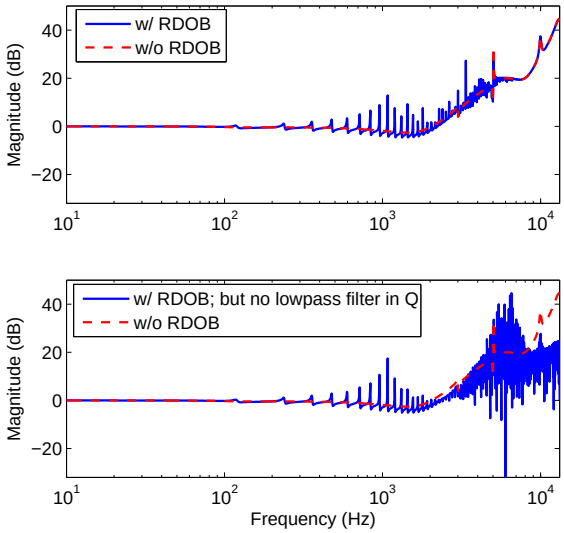

Figure 10: Magnitude responses of $1/T(z^{-1})$, which define the upper bounds for plant uncertainty to preserve robust stability.

Fig. 10 shows the magnitude responses of $1/T(z^{-1})$, the inverse of the complementary sensitivity function. From (18), in order to preserve the robust stability, magnitude of the plant uncertainty has to be lower than that of $1/T(z^{-1})$ at all frequencies. From the top plot, we observe that the introduction of RDOB largely preserves the robust stability bounds (compared to the baseline closed-loop system), especially in the high-frequency region. The minimal value of the solid line is -4.7dB (0.582 in absolute value) at 1327 Hz, i.e., the plant should not have an uncertainty that is larger than 58.2% at this frequency. The necessity of the zero-phase lowpass filter $q(z,z^{-1})$ is evident from the bottom plot. Without $q(z,z^{-1})$, 3 percent (-31dB) of model uncertainty at 6000 Hz will drive the system unstable.

Simulation is conducted by applying a full set of practical disturbances that includes the disk-flutter disturbance, the sensor noise, the repeatable runout (RRO), and the input force disturbance. Fig. 11 presents the spectra of the position error signals (PES) (in the steady state) with and without RDOB. One can remark that the repetitive errors below 2000 Hz are successfully removed,[4] and that amplification of other errors is visually not distinguishable. As a performance metric in HDD industry, the 3σ (σ denotes the standard deviation) value of the PES reduces from 10.77% Track Pitch (TP) to 9.30% TP, indicating a 13.6 percent improvement.

The bottom plot of Fig. 12 shows the PES spectrum with RDOB and $\alpha = 0$, which corresponds to previous RC schemes. It is observed that the repetitive disturbance components are also significantly reduced. However, due to the amplification of the non-periodic components

[4]The multiple spectral peaks between 800 Hz and 1300 Hz are due to the non-repetitive disk-flutter disturbances.

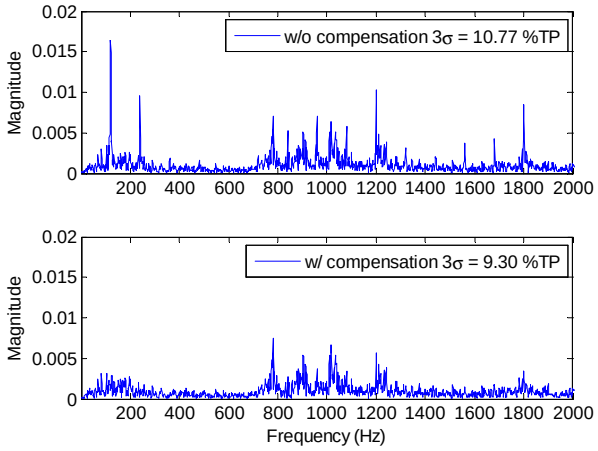

Figure 11: Spectra of PES with and without compensation.

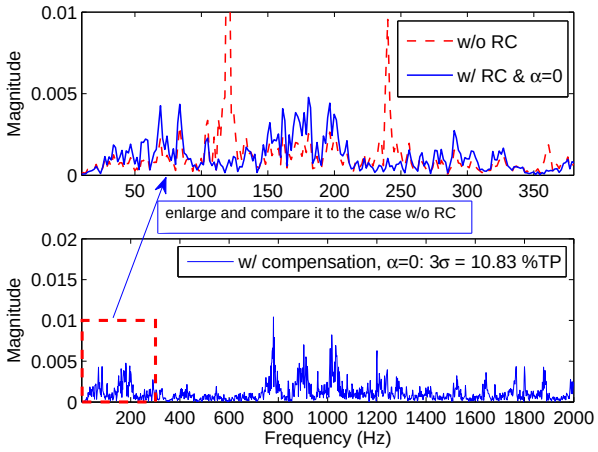

Figure 12: PES spectrum in RDOB with an FIR Q.

(see the amplified peaks compared to Fig. 11, and also the enlarged view in the top plot of Fig. 12), the overall 3σ value does not improve but is instead amplified, as can be predicted from the steady-state loop-shaping analysis in Fig. 5. In addition, to avoid excessive high-frequency disturbance amplification, the bandwidth of the zero-phase lowpass filter in $Q(z^{-1})$ has to be reduced to 1585 Hz. In this environment that consists of not only repetitive but also a significant amount of non-repetitive disturbances, a conventional RC has experienced difficulty improving the overall regulation performance.

To investigate further the transient performance, next we provide simulation results using an additional disturbance profile that is richer in repetitive components. Figs. 13 and 14 demonstrate time traces of PES using different configurations of α in $Q(z^{-1})$. In all cases, the baseline feedback loop has been running for 3 revolutions before RDOB is turned on. In Fig. 13, α maintains at 0.999 in the top plot throughout the simulation, and is configured to exponentially decay from 1 to 0.999, at the rate of 0.9/sample in the bottom plot. We observe that the

dynamic switching algorithm provides a much smoother transient response with no visually distinguishable overshoots.[5]

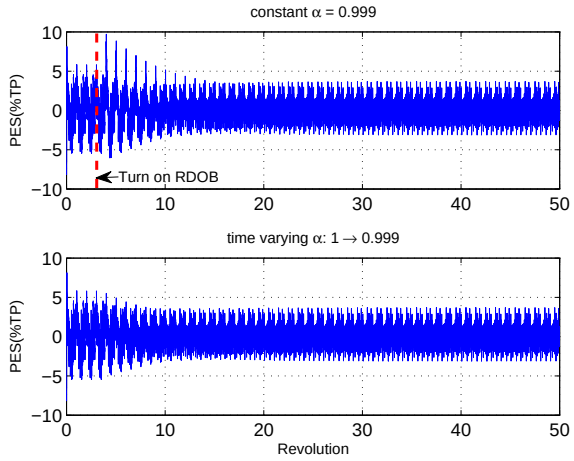

Figure 13: Comparison of the transient responses with and without the time-varying α in $Q(z^{-1})$.

In the top plot of Fig. 14, the final value of the time-varying α is chosen as 0.99. Compared to the bottom plot of Fig. 13, we can see that a smaller α yields shorter transient response, as predicted by the analysis in Section V. More specifically, the time constants (defined by (20)) for $\alpha = 0.999$ and 0.99 are respectively 4.5432 and 0.4523 revolutions. One can observe from Fig. 13 and the top plot of Fig. 14, that the transient durations are indeed about 4.5 and 0.5 revolutions, in agreement with what have just been computed from (20). Note that $\alpha = 0.99$ yields worse disturbance rejection results at the steady state. This is supported by the analysis in Section II-B. One way to balance the performance is to let α first reduce quickly from 1 to 0.99, and then gradually increase to the final value 0.999, as shown in Fig. 15. The bottom plot of Fig. 14 depicts the achieved PES time trace using such a configuration.

B. Application to tracking control on a wafer-scanner system

Besides regulation control, the proposed algorithm has also been implemented in tracking control on a laboratory testbed of an industrial wafer scanner. Such devices are essential for manufacturing integrated circuits in the semiconductor industry. The wafer scanner operates by repeatedly following a designed reference trajectory. A picture of the setup is shown in Fig. 16. There are two stages in the system, mounted on air bearings and actuated by epoxy-core linear permanent magnet motors (LPMMs). The stage positions are measured by laser interferometers. A LabVIEW real-time system with field-programmable gate array (FPGA) is used to execute the control commands with a sampling time of 0.0004 sec.

[5]The peaking phenomenon in the top plot comes from the closed-loop dynamics. By checking the dynamics of $P/(1+PC)$, one can verify that the impulse and step responses from the RDOB output to $e(k)$ have large peak values.

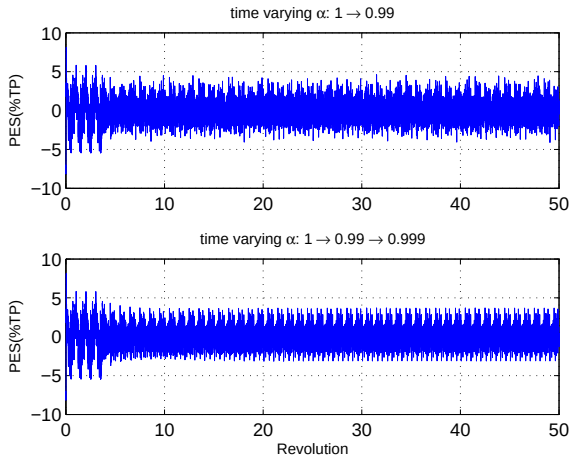

Figure 14: Comparison of the transient responses w.r.t. different configurations of time-varying α's.

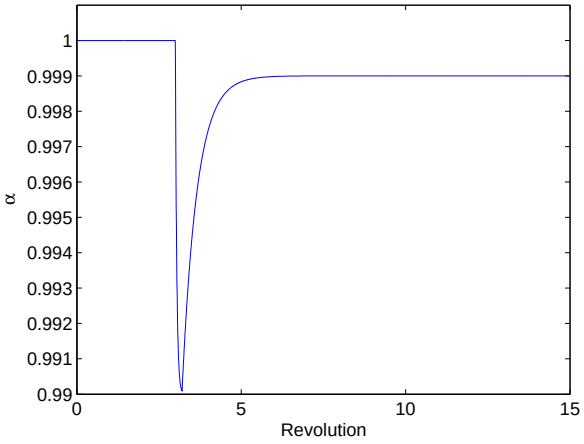

Figure 15: Time traces of α to achieve the bottom plot in Fig. 14.

The top stage is used for verification of the proposed algorithm. The system has a nominal model given by

$$z^{-m}P_n(z^{-1}) = z^{-2}\frac{3.4766\times10^{-7}(1+0.8z^{-1})}{(1-z^{-1})^2}$$

with the baseline feedback controller being a simple

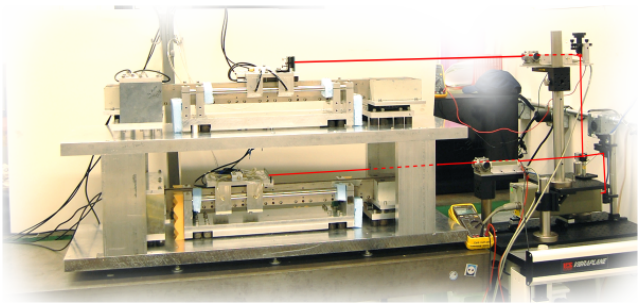

Figure 16: A testbed of an industrial wafer-scanner system.

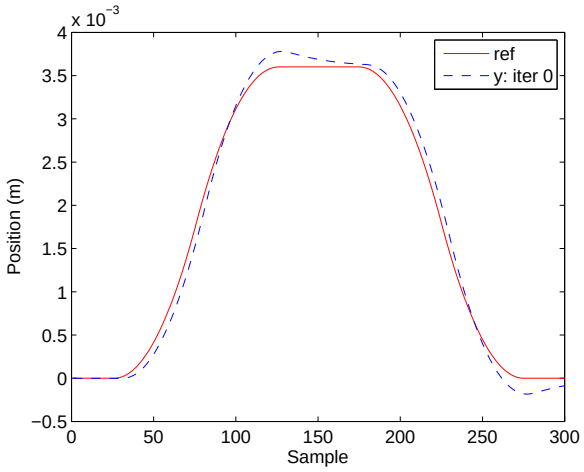

Figure 17: Reference trajectory and the actual wafer-stage position without repetitive control.

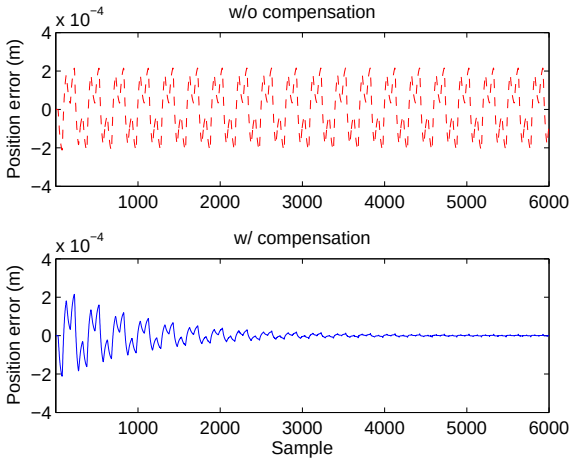

Figure 18: Tracking errors with RDOB but without transient control.

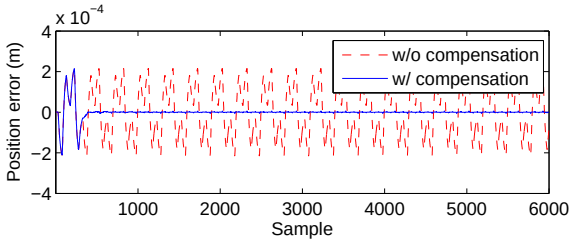

Figure 19: Tracking errors with RDOB and transient control.

PID controller. The applied reference trajectory is as shown by the solid line in Fig. 17. The dashed line in Fig. 17 shows the tracking result when we apply only the baseline feedback controller. For the resulting tracking errors, the 3σ value is 3.814×10^{-4} m. By the nature of the process, the trajectory is repeatedly applied. Fig. 18 presents the experimental results of the tracking errors for the first twenty repetitions, where the top and the bottom plots provide respectively the position errors without repetitive control and with the proposed algorithm. No transient control for α is applied in Fig. 18. We can observe that repetitive control has greatly reduced the tracking errors at the steady state. The 3σ value reduces from 3.814×10^{-4} m at the first repetition to 4.160×10^{-6} m at the 20^{th} repetition, indicating a 99.7% reduction. The proposed algorithm in Section V is then applied to additionally accelerate the transient response. Fig. 19 shows the results for RDOB with transient control. Comparing the results with that in Fig. 18, we can see that the transient duration has been significantly reduced while at the same time the steady-state performance has been preserved.

To compare the performance of the proposed algorithm with that of a conventional RC, a reference trajectory that consists of four sinusoidal components at 20, 40, 60, and 80 Hz is tested. Additionally a random disturbance obeying a normal distribution is applied to the system to examine the performance of the algorithms under noisy environments. Fig. 20 shows the spectra of the resulting tracking errors. It is seen from the first subplot that without repetitive control, large peaks appear at 20, 40, 60, and 80 Hz in the tracking-error spectrum. Using a conventional RC ($\alpha=0$), spectral peaks at the repetitive frequencies are removed as shown in the middle plot. However, since all error components in the previous repetition are applied, the non-repetitive errors can be seen to have increased (see the additional spectral peaks at the non-repetitive frequencies). This corresponds well to the loop-shaping results in Fig. 5. In the proposed scheme, only the repetitive components are reduced, and no visual amplification of the non-repetitive disturbances is observed. A similar comparison can be made in the time domain, where we see from Fig. 21 that the amplification of the non-repetitive errors has actually increased the overall error magnitude.

VII. Conclusion and future work

In this paper, we have discussed a new repetitive control scheme using the structure of a disturbance observer. From the disturbance-observer perspective, the conventional configuration is extended to address a general class of disturbance spectrum. From the repetitive-control perspective, a new implementation of the internal model principle is proposed, with a corresponding loop-shaping design criteria that enables improved loop shapes. This has an important advantage during rejecting repetitive disturbances or following repetitive trajectories when the system is additionally subjected to non-repetitive disturbances. A dynamic switching algorithm is proposed and has been shown to effectively improve the transient performance.

The proposed scheme requires knowledge of the period of the repetitive disturbance/reference. In situations where the period (order of the internal model) is unknown or uncertain, online identification and adaptation are required. Future works include identifying the

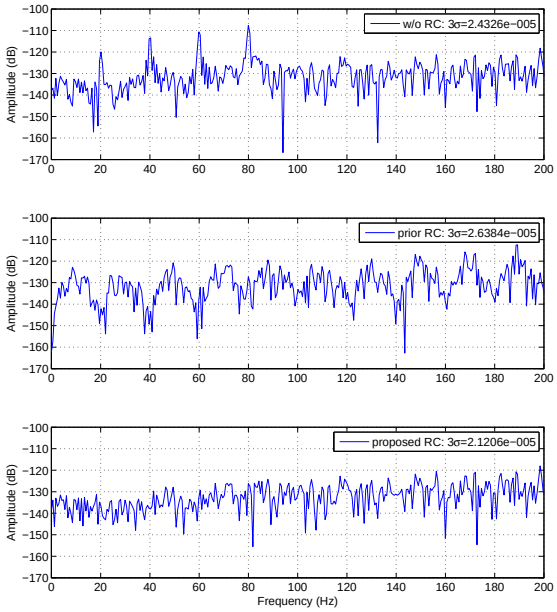

Figure 20: Spectra of the tracking errors under different RC schemes.

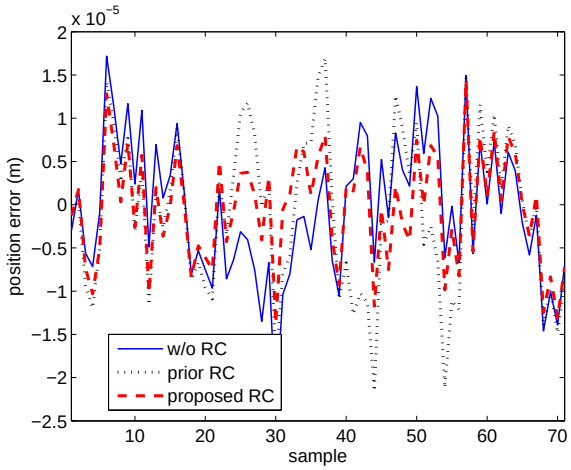

Figure 21: A section of the time trace of the tracking errors under different RC schemes.

internal-model order and analyzing the resulted transient response.

Finally we note that in a plug-in (ideal-case) repetitive control scheme, if we apply $\alpha z^{-N}/(1-z^{-N})$ parallel to the baseline controller $C(z^{-1})$, we get the following overall feedback controller and the corresponding sensitivity function:

$$C_{eq}(z^{-1}) = C(z^{-1}) + \frac{\alpha z^{-N}}{1-z^{-N}}$$

$$S(z^{-1}) = \frac{1-z^{-N}}{(1-z^{-N})[1+P(z^{-1})C(z^{-1})] + \alpha z^{-N} P(z^{-1})}.$$

Here α is a scaling factor. If $\alpha = 0$, no modification is made to the closed-loop system; if $\alpha \neq 0$, we have high-gain control at the frequencies (denoted as $\{\omega_i\}_{i=0}^{N-1}$) of the roots of $1-z^{-N}=0$, and the internal model $1-z^{-N}$ is absorbed in $S(z^{-1})$. Specifically we can make α small such that $\alpha z^{-N}/(1-z^{-N})$ has low magnitude at all frquencies other than $\omega \in \{\omega_i\}_{i=0}^{N-1}$, while in the meantime $1-z^{-N}$ still operates to cancel the repetitive errors in $S(z^{-1})$. The structure of $S(z^{-1})$ and the closed-loop properties (such as the stability condition) are different from those defined by (5) and (11). Yet this type of small-gain plug-in repetitive control can also create loop shapes that are similar to what we have discussed in the paper.

Acknowledgment

The authors thank Dr. Hoday Stearns for her help in setting up the experiments. The authors would also like to thank Prof. Tsu-Chin Tsao for presenting the small-gain plug-in repetitive control idea.

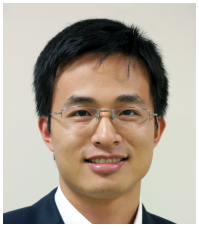

Xu Chen received his B.S. degree in 2008 from Tsinghua University, China, and his M.S. degree from UC Berkeley in 2010, both in Mechanical Engineering. He is currently pursuing the Ph.D. degree in Mechanical Engineering, University of California at Berkeley.
His research interests include adaptive control, optimization-based control, repetitive and iterative learning control, inverse control, vibration rejection, delay compensation, and digital filter design.
Xu Chen is the 2008 Excellent College Graduate of Tsinghua University, with the undergraduate thesis selected as 2008 Excellent Undergraduate Thesis of Tsinghua University. He was a recipient of the 2012 Chinese Government Award for Outstanding Self-financed Students Abroad and the 2011 Frank and Margaret Lucas Scholarship at UC Berkeley.

Masayoshi Tomizuka received his B.S. and M.S. degrees in Mechanical Engineering from Keio University, Japan and his Ph. D. degree in Mechanical Engineering from MIT in 1974. He joined the Department of Mechanical Engineering at the University of California at Berkeley in 1974, where he currently is the Cheryl and John Neerhout, Jr., Distinguished Professor.
Dr. Tomizuka teaches courses in dynamic systems and controls and conducts research on optimal and adaptive control, digital control, motion control, and their applications to robotics, manufacturing, information storage devices and vehicles. He served as Program Director of the Dynamic Systems and Control Program of the Civil and Mechanical Systems Division of NSF (2002-2004). He was Technical Editor of the ASME Journal of Dynamic Systems, Measurement and Control (1988-93), and Editor-in-Chief of the IEEE/ASME Transactions on Mechatronics (1997-99). He is a Fellow of ASME, IEEE, the International Federation of Automatic Control (IFAC) and the Society of Manufacturing Engineers. He is the recipient of the Charles Russ Richards Memorial Award (ASME, 1997), the Rufus Oldenburger Medal (ASME, 2002) and the John R. Ragazzini Award (American Automatic Control Council, 2006).

References

[1] B. A. Francis and W. M. Wonham, "The internal model principle for linear multivariable regulators," *Applied Mathematics & Optimization*, vol. 2, no. 2, pp. 170–194, Jun. 1975.

[2] T. K. S. M. T. Inoue, M. Nakano and H. Baba, "High accuracy control of a proton synchrotron magnet power supply," in *Proc. IFAC World Congress*, 1981, pp. 3137–3142.

[3] S. Hara, Y. Yamamoto, T. Omata, and M. Nakano, "Repetitive control system: a new type servo system for periodic exogenous signals," *IEEE Trans. Autom. Control*, vol. 33, no. 7, pp. 659 –668, Jul 1988.

[4] M. Tomizuka, T.-C. Tsao, and K.-K. Chew, "Analysis and synthesis of discrete-time repetitive controllers," *ASME Journal of Dynamic Systems, Measurement, and Control*, vol. 111, no. 3, pp. 353–358, 1989.

[5] G. Hillerström and K. Walgama, "Repetitive control theory and applications-a survey," in *Proc. 13th IFAC World Congress*, 1996, pp. 1–6.

[6] C. Li, D. Zhang, and X. Zhuang, "A survey of repetitive control," in *Proc. 2004 IEEE/RSJ International Conf. on Intelligent Robots and Systems*, vol. 16, no. 7, Jan. 2004, pp. 1160 – 1166.

[7] K. Chew and M. Tomizuka, "Digital control of repetitive errors in disk drive systems," *IEEE Control Syst. Mag.*, vol. 10, no. 1, pp. 16–20, 1990.

[8] J. Moon, M. Lee, and M. Chung, "Repetitive control for the track-following servo system of an optical disk drive," *IEEE Trans. Control Syst. Technol.*, vol. 6, no. 5, pp. 663–670, 2002.

[9] Y. Onuki and H. Ishioka, "Compensation for repeatable tracking errors in hard drives using discrete-time repetitive controllers," in *Proc. 6th IEEE International Workshop on Advanced Motion Control*, 2000, pp. 490–495.

[10] L. Guo, "Reducing the manufacturing costs associated with hard disk drives-a new disturbance rejection control scheme," *IEEE/ASME Trans. Mechatronics*, vol. 2, no. 2, pp. 77–85, 2002.

[11] C. Cosner, G. Anwar, and M. Tomizuka, "Plug in repetitive control for industrial robotic manipulators," in *Proc. 1990 IEEE International Conf. on Robotics and Automation,*, May 1990, pp. 1970 –1975 vol.3.

[12] R. W. Longman, "Iterative learning control and repetitive control for engineering practice," *International Journal of Control*, vol. 73, no. 10, pp. 930–954, 2000.

[13] T. Doh, J. Ryoo, and M. Chung, "Design of a repetitive controller: an application to the track-following servo system of optical disk drives," in *IEE Proc. Control Theory and Applications*, vol. 153, no. 3. IET, 2006, pp. 323–330.

[14] T. Inoue, "Practical repetitive control system design," in *Proc. 29th IEEE Conf. on Decision and Control*, Dec 1990, pp. 1673 –1678 vol.3.

[15] K. Srinivasan and F.-R. Shaw, "Analysis and design of repetitive control systems using the regeneration spectrum," in *Proc. American Control Conf.*, May 1990, pp. 1150 –1155.

[16] M.-C. Tsai and W.-S. Yao, "Design of a plug-in type repetitive controller for periodic inputs," *IEEE Trans. Control Syst. Technol.*, vol. 10, no. 4, pp. 547 –555, jul 2002.

[17] M. Tomizuka, "Dealing with periodic disturbances in controls of mechanical systems," *Annual Reviews in Control*, vol. 32, no. 2, pp. 193 – 199, 2008.

[18] ——, "Zero phase error tracking algorithm for digital control," *ASME Journal of Dynamic Systems, Measurements, and Control*, vol. 109, no. 1, pp. 65–68, 1987.

[19] M. Steinbuch, S. Weiland, and T. Singh, "Design of noise and period-time robust high-order repetitive control, with application to optical storage," *Automatica*, vol. 43, no. 12, pp. 2086–2095, 2007.

[20] G. Pipeleers, B. Demeulenaere, J. De Schutter, and J. Swevers, "Robust high-order repetitive control: optimal performance trade-offs," *Automatica*, vol. 44, no. 10, pp. 2628–2634, 2008.

[21] J. C. Doyle, B. A. Francis, and A. Tannenbaum, *Feedback control theory*. Macmillan, 1992, vol. 134.

[22] R. Ehrlich and D. Curran, "Major HDD TMR sources and projected scaling with TPI," *IEEE Trans. Magn.*, vol. 35, no. 2, pp. 885–891, Mar 1999.

[23] K. Ohnishi, "Robust motion control by disturbance observer," *Journal of the Robotics Society of Japan*, vol. 11, no. 4, pp. 486–493, 1993.

[24] C. J. Kempf and S. Kobayashi, "Disturbance observer and feed-forward design for a high-speed direct-drive positioning table," *IEEE Trans. Control Syst. Technol.*, vol. 7, no. 5, pp. 513–526, 1999.

[25] M. White, M. Tomizuka, and C. Smith, "Improved track following in magnetic disk drives using a disturbance observer," *IEEE/ASME Trans. Mechatronics*, vol. 5, no. 1, pp. 3–11, Mar. 2000.

[26] K. S. Eom, I. H. Suh, and W. K. Chung, "Disturbance observer based path tracking control of robot manipulator considering torque saturation," *Mechatronics*, vol. 11, no. 3, pp. 325 – 343, 2001.

[27] K. K. Tan, T. H. Lee, H. F. Dou, S. J. Chin, and S. Zhao, "Precision motion control with disturbance observer for pulsewidth-modulated-driven permanent-magnet linear motors," *IEEE Trans. Magn.*, vol. 39, no. 3, pp. 1813–1818, 2003.

[28] K. Yang, Y. Choi, and W. K. Chung, "On the tracking performance improvement of optical disk drive servo systems using error-based disturbance observer," *IEEE Trans. Ind. Electron.*, vol. 52, no. 1, pp. 270–279, Feb. 2005.

[29] X. Chen and M. Tomizuka, "An enhanced repetitive control algorithm using the structure of disturbance observer," in *Proc. 2012 IEEE/ASME International Conf. on Advanced Intelligent Mechatronics (AIM)*, July 2012, pp. 490 –495.

[30] H. S. Lee and M. Tomizuka, "Robust motion controller design for high-accuracy positioning systems," *IEEE Trans. Ind. Electron.*, vol. 43, no. 1, pp. 48 –55, feb 1996.

[31] K. Astrom, P. Hagander, and J. Sternby, "Zeros of sampled systems," *Automatica*, vol. 20, no. 1, pp. 31 – 38, 1984.

[32] S. Skogestad and I. Postlethwaite, *Multivariable Feedback Control: Analysis and Design*, 2nd ed. Wiley Chichester, UK, 2005.

[33] H. Dotsch, H. Smakman, P. Van den Hof, and M. Steinbuch, "Adaptive repetitive control of a compact disc mechanism," in *Proc. 34th IEEE Conf. on Decision and Control, 1995*, vol. 2. IEEE, 1995, pp. 1720–1725.

[34] D. Liberzon and A. Morse, "Basic problems in stability and design of switched systems," *IEEE Control Syst. Mag.*, vol. 19, no. 5, pp. 59–70, 1999.

[35] IEEJ, Technical Commitee for Novel Nanoscale Servo Control, "NSS benchmark problem of hard disk drive systems," http://mizugaki.iis.u-tokyo.ac.jp/nss/, 2007.